Jurnal Teknologi

Full Paper

THE CT NUMBER UNIFORMITY AND HOMOGENEITY: WHICH IS BETTER FOR DETECTING THE BEAM HARDENING ARTEFACTS?

Choirul Anam[a], Riska Amilia[a], Ariij Naufal[a], Anisa T. Maya[b], Yanurita Dwihapsari[c]

[a]Department of Physics, Faculty of Sciences and Mathematics, Diponegoro University, 50275, Central Java, Indonesia
[b]Loka Pengamanan Fasilitas Kesehatan (LPFK) Surakarta, Mojosongo, Jebres, Surakarta City 57127, Central Java, Indonesia
[c]Department of Physics, Faculty of Science and Data Analytics, Institut Teknologi Sepuluh Nopember, Kampus ITS Sukolilo – Surabaya 60111, East Java, Indonesia

Article history
Received
18 January 2024
Received in revised form
6 May 2024
Accepted
12 May 2024
Published Online
20 February 2025

*Corresponding author
anam@fisika.fsm.undip.ac.id

Graphical abstract

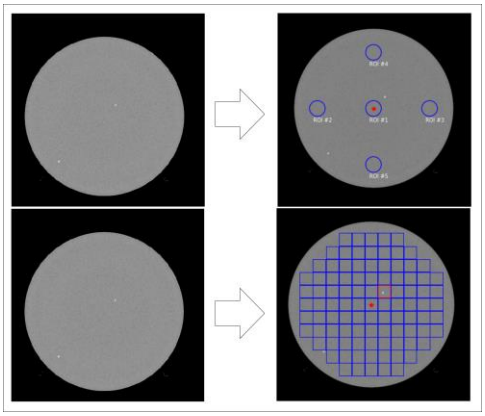

Abstract

This study compares the CT number uniformity and homogeneity for detecting beam hardening artefact from images of the American College of Radiology (ACR) computed tomography (CT) phantom scanned with 20 CT scanners from four manufacturers, and images with and without beam hardening artefact. Software to automatically measure CT number uniformity and homogeneity was developed. For CT number uniformity, the coordinates of the peripheral positions of the region of interest (ROIs) at four different positions and one ROI at the middle of the phantom were automatically determined. For CT number homogeneity, the rectangular ROIs of 32 pixels across 85% of the area of the phantom were automatically arranged. CT number uniformity and homogeneity of images from 20 CT scanners were investigated using an ACR CT phantom. To find usefulness of the CT number homogeneity, images with and without beam hardening artefacts were evaluated. The developed software successfully measured CT number uniformity and homogeneity of the images. All scanners produced achievable range of CT number uniformity, i.e., within 5 HU. However, some scanners had CT number homogeneities less than 5 HU, while others had CT number homogeneities more than 5 HU. It is found that the CT number homogeneity is able to detect the beam hardening artefact, while CT number uniformity is not able to detect it. A system for automatically measure CT number uniformity and homogeneity has been developed. The developed system is easy to implement and human-observer independent. CT number homogeneity is more sensitive for detecting beam hardening artefact than CT number uniformity.

Keywords: CT number linearity, Catphan phantom, CT scan, image quality

1.0 INTRODUCTION

Using computed tomography (CT) scans as an imaging modality is burgeoning for patient diagnosis across all ages [1-5]. It is due to the tremendous capability of CT to represent any detail part of a patient's body, including blood vessels, bones, and other organs [6-9]. It is noted that many factors, directly or indirectly, affect CT image quality [10-13]. Image quality is essential to CT application since a low-quality CT image can lead to negative or positive false diagnosis [14,15].

Unfortunately, a CT image is vulnerable to artefacts, a condition where the pixel values or CT numbers in an image differ from the accurate attenuation coefficients of the object [16,17]. Many types of artefacts commonly appear; one of them is beam hardening artefact, which occurs when the low-energy X-ray is absorbed more rapidly than the high-energy X-ray by an object [18-20]. Another artefact common in CT images is a ring artefact, emerged as an impact of mis-calibration or a detector defect [21-23]. These or other artefacts can lead to an inhomogeneity of CT numbers within an image across the field of view (FOV) and potentially decrease image quality to a lower-than-appropriate level for diagnostic requirements [24]. For this reason, an attempt to detect and minimize artefacts must be taken.

Due to the potential existence of artefacts, testing the CT number uniformity is essential in the quality control program. Evaluating the CT number uniformity aims to detect the non-uniformities of measured CT numbers, which hamper the production of a free-artefacts image [25,26]. The test was carried out by analysing the difference in average CT number at the centre and periphery of the homogenous phantom, with the established tolerances (i.e., 4 HU according to International Electrotechnical Commission (IEC) [27] and 5 HU according to ACR recommendation [28]).

However, under certain circumstances, the CT number uniformity test may only detect the presence of artefacts partially because the measurements are limited only at five points. For generating a more accurate detection of artefacts, a CT number homogeneity test is introduced by Nowik *et al*. [29]. Compared to the CT number uniformity, the CT number homogeneity evaluation may provide additional sensitivity to some artefacts because the measurement is carried out with broader regions of interest (ROI) across the image [29]. Unfortunately, the measurement of CT number homogeneity needs special dedicated software, which is not always be available at every medical centers. In addition, comprehensive and comparative studies on CT number uniformity and homogeneity comparisons for detecting the beam hardening artefacts are limited to date. Therefore, based on the mentioned problems, this study aims to develop software to automatically measure CT number uniformity and homogeneity, and to compare the CT number uniformity and homogeneity for detecting the beam hardening artefacts on American College of Radiology (ACR) CT phantom images scanned using 20 different CT scanners and images reconstructed with and without beam hardening artefacts.

2.0 METHODOLOGY

2.1 Automated CT Number Uniformity Measurement

In this study, CT number uniformity measurement was automatically performed. The measurement for automatic measurement of CT number uniformity was initiated by opening the phantom image and converting the pixel values from CT data to Hounsfield units (HU). Since this study only focuses on CT number uniformity testing, the third module of ACR CT phantom was used, as shown in Figure 1(a). Next, the image was segmented with a threshold value of -200 HU to obtain a binary image, and its midpoint was determined and presented by Figure 1(b). The radius of the binary image was measured to determine the coordinates at peripheral positions, as shown in Figure 1(c). Then, the coordinates of the peripheral positions at four different positions, 3, 6, 9, and 12 o'clock, were determined with a distance of 60 pixels from the phantom's edge; a total of 5 coordinate points were obtained, one in the middle and four on the edge of the phantom (Figure 1(d)). A circular ROI with a diameter of 40 pixels was created from each point, as shown in Figure 1(e).

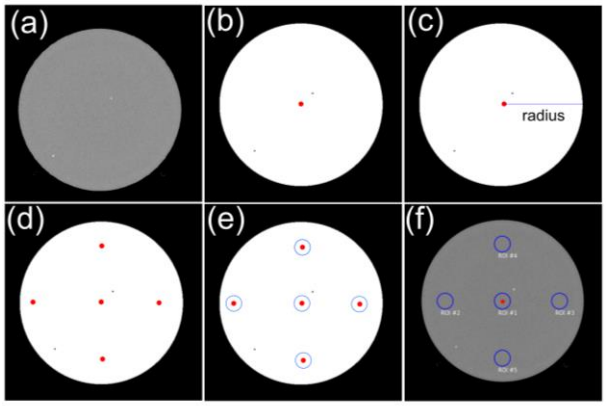

Figure 1 Steps for automatic measurement of CT number uniformity: (a) original image, (b) segmentation result of the phantom after thresholding and centroid determination, (c) measurement of phantom's radius, (d) determination of peripheral's coordinates by 60 pixels from the edge, (e) creation of ROIs with diameter of 40 pixels in each coordinate, and (f) All ROIs within the original image.

Average values of the CT numbers for each ROI were calculated (Figure 1(f)) and the CT number uniformity of the image was obtained using Equation (1):

$$CT_u = \max\left(\left|\Delta\left(\overline{CT_c} - \overline{CT_p}\right)\right|\right) \quad (1)$$

where $\overline{CT_c}$ is the average CT number from the central ROI and $\overline{CT_p}$ is the average CT number from each peripheral ROI.

A system for automatic measurement of CT number uniformity was integrated into IndoQCT software [30], and its screenshot is depicted by Figure 2. The tolerance level based on ACR recommendation, i.e., 5 HU for achievable value [28], was displayed.

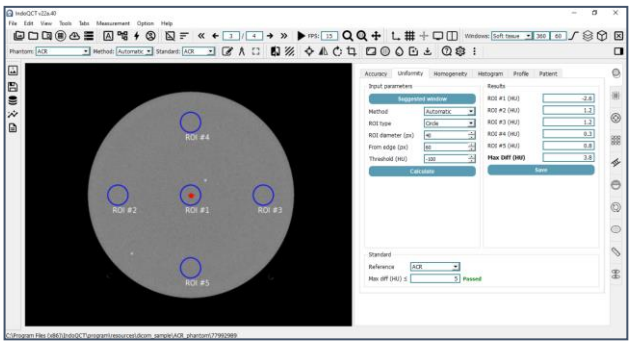

Figure 2 The displayed IndoQCT for measuring CT number uniformity

2.2 Automated CT number homogeneity measurement

CT number homogeneity measurement was also automatically carried out. In this study, a software for measuring CT number homogeneity was developed. In general, the initial steps of its measurement are similar to the CT number uniformity. First, the image of the third module of the ACR CT phantom was opened (Figure 3(a)). After that, the image was segmented, its center was determined, and the radius of the phantom (r_1) was automatically calculated (Figure 3(b)). Next, the primary step of CT number homogeneity measurement was ready to be performed. It is noted that instead of using five circular ROIs to measure the homogeneity, such as CT number uniformity measurement, the CT number homogeneity employed the rectangular ROIs, which were arranged continuously on the area of the phantom due to a higher coverage provided with the rectangular ROI. However, it was conducted only on 85% of the phantom area. Hence, a circular mask with a diameter of 85% of the phantom's diameter was created to assist the ROIs placement, as shown in Figure 3(c). Then, the rectangular ROIs were arranged continuously on a circular mask area (Figure 3(d)), which utilized an ROI of 32 × 32 pixels.

In case if the ROIs were at the two point locations (these two points are generally used for measuring distance accuracy and modulation transfer function), then the ROIs would be eliminated from the further steps and it was signed with a red ROI (Figure 3(e)). On ACR CT phantom, the two points are tungsten-based, hence their mean CT numbers are higher than 100 HU and the presence of the two points can be identified from the values of these CT numbers. The next step was determining the mean CT number from each ROIs within the image (Figure 3f) to obtain the maximum CT number ($\overline{CT_{max}}$) and minimum CT number ($\overline{CT_{min}}$). Finally, the CT number homogeneity (CT_h) was acquired from Equation (2).

$$CT_h = \left|\Delta\left(\overline{CT_{max}} - \overline{CT_{min}}\right)\right| \quad (2)$$

The screenshot of IndoQCT for CT number homogeneity measurement is shown in Figure 4.

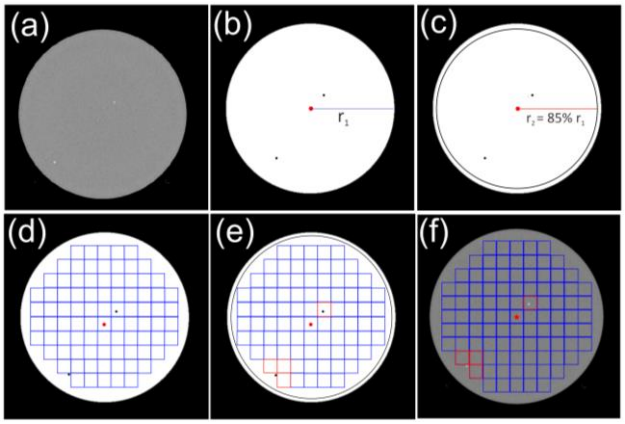

Figure 3 Steps for automatic measurement of CT number homogeneity: (a) original image, (b) result of phantom segmentation and radius measurement, (c) circular mask of 85% area of the phantom, (d) creation of contiguous rectangular ROIs within circular area, (e) all ROIs with elimination of ROIs with red boxes (due to the presence of BBs), and (f) all ROIs within the original image

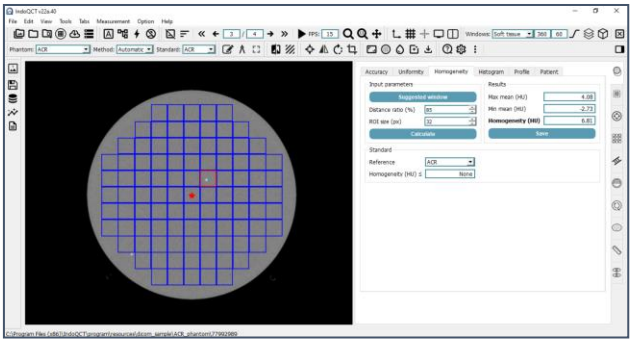

Figure 4 The displayed graphical user interface (GUI) of IndoQCT in measuring CT number homogeneity. The maximum and minimum average of CT number from each ROI, and inhomogeneity of CT number are displayed on the right side

Table 1 The input scan parameters for 20 CT scanners used in this study

No	Vendor	Scanner	kV	mA	Revolution time (s)	FOV (mm)	Slice thickness (mm)	Mode	Pitch	Convolution kernel
1	GE	Revolution ACTs	120	200	2	250	10	Axial	-	SOFT
2	GE	Revolution EVO	120	120	2	233	5	Axial	-	STANDARD
3	GE	Discovery LS	120	250	1	240	5	Axial	-	STANDARD
4	GE	Revolution EVO	120	200	0.8	235	1.25	Spiral	0.531	STANDARD
5	GE	LightSpeed	120	250		240	5	Axial	-	STANDARD
6	GE	BrightSpeed	120	300	1	204	10	Axial	-	STANDARD
7	GE	Revolution EVO	120	160	1.46	235	9	Spiral	0.75	STANDARD
8	GE	Brivo CT325	120	200	1	250	10	Axial	-	STD+
9	GE	Revolution ACTs	120	200	1	237	10	Spiral	0.875	SOFT
10	GE	Revolution EVO	120	160	1	235	5	Spiral	0.531	STANDARD
11	Hitachi	Eclos	120	175	2	220	10	Axial	-	12
12	Hitachi	Eclos	120	175	2	220	10	Axial	-	12
13	Hitachi	Supria	120	200	1	208	10	Axial	-	11
14	Hitachi	Supria	120	178	1	204	1.25	Axial	-	12
15	Hitachi	Eclos	120	300	1	210	10	Axial		10
16	Siemens	Emotion 16	130	180	1.5	226	5	Spiral	0.6	H31s
17	Siemens	Somatom go.Now	130	118	1.67	200	8	Spiral	0.6	Hr36f
18	Siemens	Emotion 16	130	132	1	211	5	Spiral	0.6	H31s
19	Toshiba	Alexion	120	200	1	209	5	Spiral	0.689	FC26
20	Toshiba	Alexion	120	150	1.5	220	10	Spiral	0.688	FC68

2.3 Phantom Images

Comparison of CT number uniformity and homogeneity for detecting the beam hardening artefacts will be carried out on an ACR 464 CT phantom from Gammex Inc, USA. The ACR CT phantom consists of four separate modules. CT number uniformity and homogeneity evaluation were performed on the third module composed by a uniform solid-water object with CT number around 0 HU. This module also contains two tiny cube's radiopaque balls (BB) from tungsten ($Z \approx 74$) for measuring modulation transfer function (MTF) and distance accuracy.

ACR phantom was scanned by 20 CT scanners, which were tabulated in Table 1. The employed scanners were manufactured by four different vendors: 10 scanners from GE, five scanners from Hitachi, three scanners from Siemens, and two scanners from Toshiba. The examinations were performed with adult abdomen protocol with the disabled auto mA feature following the recommendation of ACR.

To indicate usefulness of the CT number homogeneity for detecting the beam hardening artefacts over CT number uniformity, we applied both parameters to images with beam hardening artefact. The Siemens phantom was 20-cm in diameter. The phantom was made from homogeneous water with an acrylic outer. The phantom was scanned with a Siemens Somatom go Now CT scanner with imaging parameters: tube voltage 130 kV, tube current 80 mA, slice thickness 5 mm, FOV 258mm, rotation time 1 s, and pitch 0.45. The image was reconstructed using the Filtered-Back Projection (FBP) with beam hardening artefact. To remove the beam hardening artefact, the reconstructed image with FBP was added with Iterative Beam-Hardening Correction (IBHC) method.

4.0 RESULT AND DISCUSSION

The results of automatic ROI placement for 20 CT scanners on CT number uniformity measurements are exhibited by Figure 5. As can be seen, a large FOV used in images #1, #4, #6, and #7 did not affect the placement of the ROI performed. In addition, the presence of truncated images due to the smaller FOVs on scanners #5, #10, #11, #12, #14, and #17 did not interrupt the segmentation, and the results obtained were still optimal. Furthermore, the variation of input parameter settings also did not influence the ROI placement. The ROIs able to be arranged accurately across all images regardless the large or small FOVs employed.

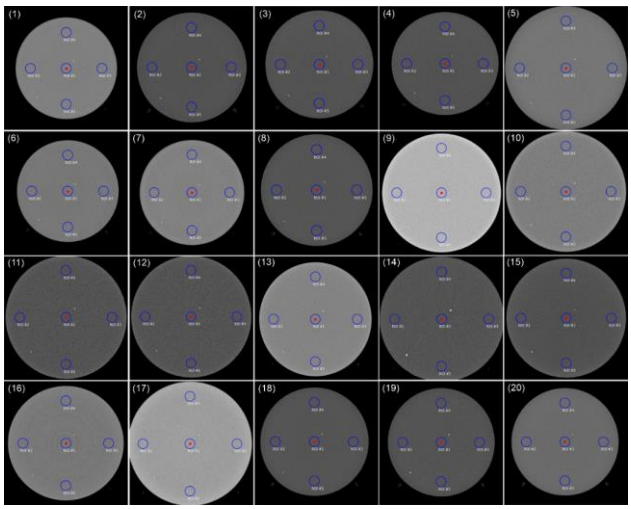

Figure 5 Automatic segmentation result of ACR 464 CT phantom from 20 CT scanners in measurement of CT number uniformity

The results of CT number uniformity across all scanners are shown in Figure 6. Overall, all scanners were in the achievable range of CT number uniformities, with the highest CT number uniformity displayed by scanner #5 from GE and the lowest value belonging to scanner #11 from Hitachi. The GE scanners produce a relatively broad values from 0.8 HU to 4.3 HU. Likewise, the Hitachi and Toshiba scanners also had a wide range from -0.6 HU to 3 HU and from 1.17 HU to 3.67 HU. At the same time, the Siemens CT scanners exhibited a minimal fluctuation, i.e., only about 0.6 HU.

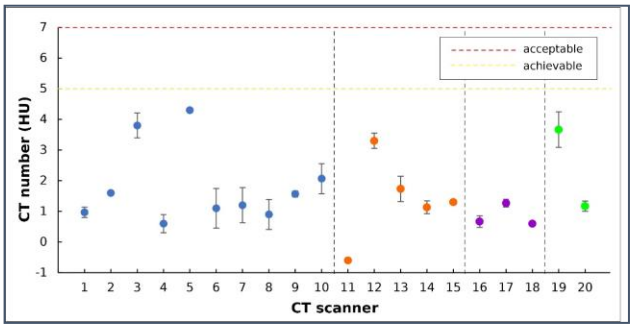

Figure 6 The CT number uniformity from 20 CT scanners. Each manufacture is represented by different colours with blue for GE, orange for Hitachi, purple for Siemens, and green for Toshiba

The CT number homogeneity measurement results are depicted in Figure 7. The ROIs still be arranged accurately on every image constructed by either large or small FOVs regardless of input parameter settings.

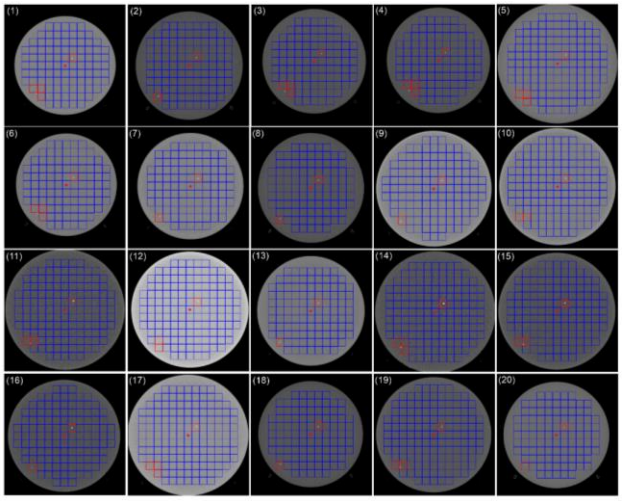

Figure 7 Automatic segmentation result of ACR 464 CT phantom from 20 CT scanners in measurement of CT number homogeneity

Figure 8 shows the CT number homogeneity measurements results from the 20 CT scanners. It is seen that most scanners (15 CT scanners) had CT number homogeneities < 5 HU, with the highest result being from scanner #19 and the lowest being from scanner #10. Scanner GE is the most used scanner in this study, yielded values from 1.72 ± 0.15 HU to 5.82 ± 0.0 HU. Two GE scanners, i.e., #3 and #5, had values above 5 HU, while the remaining GE scanners were spotted under 5 HU. Five Hitachi scanners also produced wide-range results from 2.46 HU to 4.73 HU. On the other hand, a scanner from two others, Siemens and Toshiba, yielded relatively high CT number values, i.e., 6.81 HU and 6.82 HU, respectively. The minimum value obtained from both brands was also quite high, 3.48 ± 0.24 HU for Siemens and 4.92 ± 0.05 HU for Toshiba.

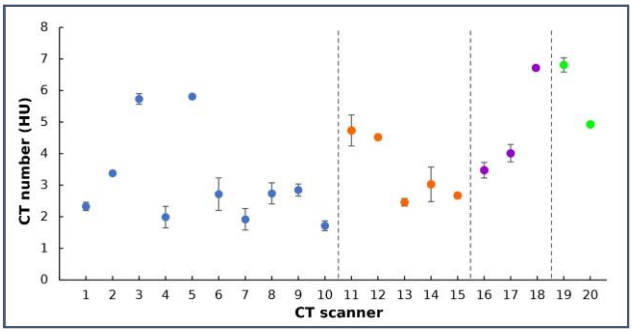

Figure 8 The CT number homogeneity from 20 CT scanners. Each manufacture is represented by different colours with blue for GE, orange for Hitachi, purple for Siemens, and green for Toshiba

Figure 9 represents the comparison of CT number homogeneity (orange) and CT number uniformity (blue). In general, the CT number homogeneity has slightly higher than CT number uniformity. A different trend was obtained on scanner # 10 where the CT number uniformity is 0.3 HU higher than the CT number homogeneity. The average difference between those two was 5% with the biggest difference was seen on scanner #18 with 6.21 HU. The smallest difference was found on scanner #10, followed by scanner #7 with 0.72 HU and scanner #13 with 0.73 HU.

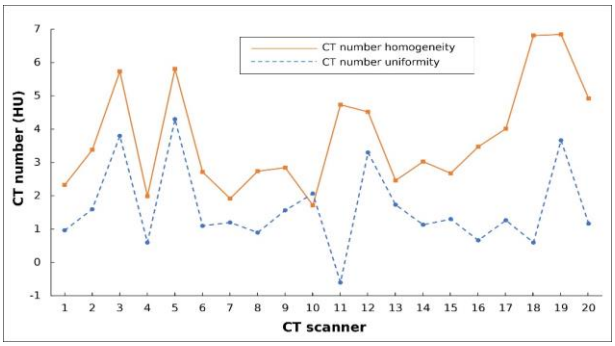

Figure 9 The line chart represents comparison of CT number homogeneity (orange) and CT number uniformity (blue)

The ROIs for CT number uniformity and homogeneity for images with and without beam hardening artefact are shown in Figure 10. Visually, it is clear that there are differences between images reconstructed with the FBP method (first row) and the FBP + IBHC method (second row). The beam hardening artefact is seen in the image reconstructed with only FBP. The periphery of the image looks lighter compared to the centre of the image which is darker. In contrast, the image reconstructed with the FBP + IBHC method is more homogeneous across all areas of the image. It important to note that the placement of ROIs in the entire image remains accurate according to the specified position either for measuring CT number uniformity and homogeneity.

The results of CT number uniformity and homogeneity are shown in Table 2. It is found that the image containing the beam hardening artefact has a CT number uniformity value less than 4 HU. This shows that the CT number uniformity failed to detect the artefact, because the CT number uniformity value is still within its achievable range. Meanwhile, the CT number homogeneity value shows a value of around 15 HU which indicates the presence of beam hardening artefact. Meanwhile, in the image reconstructed with no beam hardening artefact (i.e. reconstructed with FBP + IHBC), both the CT number uniformity and homogeneity show a low value (less than 4 HU) which indicates the absence of a beam hardening artefact. Thus, it is clear that CT number homogeneity is able to distinguish whether there is a beam hardening artefact or not, while CT number uniformity cannot yet indicate the presence of a beam hardening artefact or not.

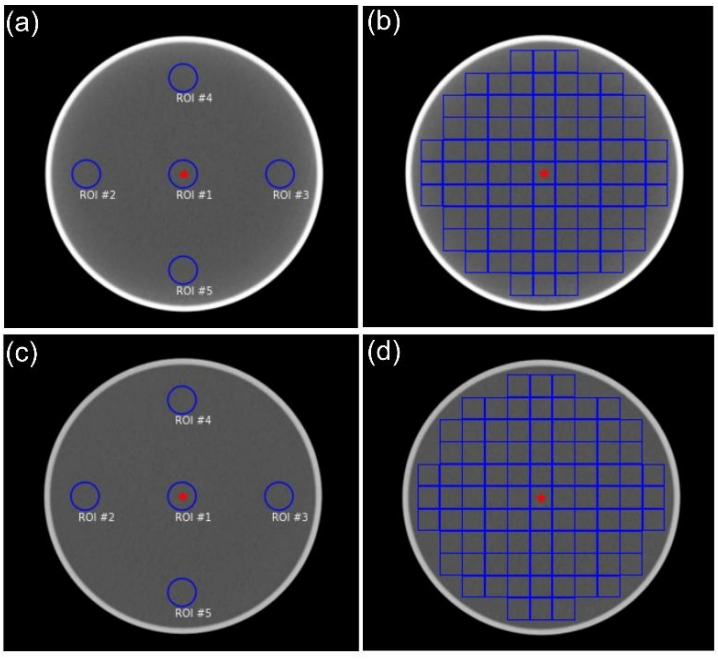

Figure 10 Siemens phantom images reconstructed with FBP method (first row) and FBP + IBHC method (second row) after measurement with CT number uniformity and CT number homogeneity

The presence of artefacts, such as beam hardening artefact, can reduce the image quality, improving diagnostic error [31]. Therefore, efforts to detect and decrease the artefact are essential. Detecting the presence of artefacts can be done by testing the uniformity and homogeneity of the CT number [25,29]. Although several software programs are already available to measure CT number uniformity automatically, the feature for measuring CT number homogeneity still needs to be improved [29]. Therefore, software to automatically measure either CT number uniformity or homogeneity is developed and evaluated in this study.

Table 2 The results of CT number uniformity and homogeneity of images reconstructed with the FBP method and the FBP + IBHC method

ROI	CT number (HU)	
	FBP	FBP + IBHC
#1	0.8 ± 0.8	0.2 ± 0.1
#2	3.8 ± 0.1	-1.0 ± 0.0
#3	3.6 ± 0.1	-1.1 ± 0.0
#4	4.4 ± 0.0	-0.4 ± 0.4
#5	3.5 ± 0.1	-0.9 ± 0.2
Uniformity	3.6 ± 0.1	0.2 ± 0.1
Max HU	14.0 ± 0.0	0.1 ± 0.1
Min HU	-1.0 ± 0.1	-2.4 ± 0.0
Homogeneity	15.0 ± 0.1	2.5 ± 0.1

The developed software succeeded in segmenting and measuring the CT number uniformity and homogeneity. Measurements were carried out quickly without any intervention from the user. The size of the FOV used and the truncated parts of the image did not disturb the segmentation and measurements. The software could still perform measurements under various image conditions and input parameters.

According to the ACR recommendations, the CT number uniformity across all scanners in this study was in the achievable range. However, there were deviations witnessed from each scanner. CT number uniformity values from scanners with the same brand can have different results. A study by Roa *et al*. [32] on 6 CT scanners showed that the CT number uniformity of the Catphan phantom was not constant. Some scanners showed a sharp fluctuation and diverge of the specified tolerance limit (> 4 HU). Study by Husby *et al*. [33] also found that the CT number uniformity value of a scanner fluctuated around 1 HU for every 100 scans.

Likewise, the CT number homogeneity from several scanners is also different. Pixel size variations show that the ROI size affected the CT number homogeneity [34]. To date, the tolerance level of CT number homogeneity is not available. The previous study only refers to the approach value. A study by Nowik *et al*. [29], for example, used a tolerance level from an initial test, which was considered reasonable, as more data are collected, systematically lower the tolerance.

In this study, CT scanners from 4 different vendors were investigated. From the results, the tolerance approach for the ACR phantom is 6 HU as an achievable level and 8 HU as an acceptable level. This is because the CT number homogeneity has slightly higher results (±5%) than the uniformity, as shown in Figure 9. The CT number homogeneity with higher coverage in areas makes it more sensitive for detecting image artefacts rather than CT number uniformity [29].

Testing the CT number uniformity and homogeneity is very important to detect the presence of artefacts in the medical images since it potentially degrades the quality of the diagnostic images. Artefact that often appear in an image is cupping artefact as impacts of the beam-hardening phenomenon. In addition, capping artefacts as a result of overcorrection sometimes appear. The appearance of these artefacts has been known as the main factor of deterministic error, enhancing the inaccuracy of diagnosis in both body and bone regions [16]. The study by Hutchinson *et al*. [36] reported that beam hardening artefact was a second challenge that complicated the diagnosis of pulmonary embolism after motion artefact.

Evaluation of CT number uniformity and homogeneity on images with and without beam hardening artefact is interesting. The CT number uniformity test on image with beam hardening artefact can only capture the CT number difference less than 4 HU. On the other hand, CT number homogeneity test on image with hardening artefact can capture CT number difference up to 15 HU. While, both CT number uniformity and homogeneity tests on image with no beam hardening artefact capture the CT number difference less than 4 HU. This indicates that CT number homogeneity can detect the presence or absence of beam hardening artefacts, while CT number uniformity cannot. However, this is only preliminary study with only one image with and without beam hardening artefact. More comprehensive testing on images with various levels of beam hardening artefacts needs to be carried out in the future so that the effectiveness and limitations of CT number homogeneity can be determined.

Another artefact that frequently emerges is a ring artefact due to the mis-calibration of the detector [16]. A study by du Plessis *et al*. [24] reported that misinterpretation of this artefact as pathology had misdiagnosed three paediatric patients initially diagnosed with tuberculous meningitis (TBM). However, evaluation of the ring artefact using the CT number uniformity and homogeneity has not been performed.

Efforts to avoid or decline the presence of artefacts have been taken to decrease the risks. Beam-hardening artefacts can be reduced by using filtration [36], patient-positioning [37,38], and the employment of a bow-tie filter [39], while ring artefacts can be reduced by conducting air calibration scan [24,31,40]. In addition, the uniformity and homogeneity test to detect the presence of the artefact can be conducted monthly according to

the International Atomic Energy Agency (IAEA) Human Health Series No. 19 [41].

4.0 CONCLUSION

The software to automatically measure CT number uniformity and homogeneity has been successfully developed. All scanners were in the achievable range of CT number uniformity, i.e., within 5 HU. Some scanners had CT number homogeneities < 5 HU, while others had CT number > 5 HU. It is found from image with beam hardening artefact that the CT number homogeneity is able to detect the artefact, while CT number uniformity is not able to detect it. Hence, it is concluded that CT number homogeneity presents a better sensitivity for detecting the beam hardening artefacts than CT number uniformity.

Acknowledgement

This work was funded by the World Class Research University (WCRU), Diponegoro University, No. 357-17/UN7.D2/PP/IV/2024.

Conflicts of Interest

The author(s) declare(s) that there is no conflict of interest regarding the publication of this paper.

References

[1] Kim, N. T., Kwon, S. S., Park, M. S., Lee, K. M., & Sung, K. H. 2022. National Trends in Pediatric CT Scans in South Korea: A Nationwide Cohort Study. *Taehan Yongsang Uihakhoe chi*. 83(1): 138–148. Doi: https://doi.org/10.3348/jksr.2021.0052.

[2] Ha, T. N., Kamarova, S., Youens, D., *et al*. 2022. Trend in CT Utilisation and Its Impact on Length of Stay, Readmission and Hospital Mortality in Western Australia Tertiary Hospitals: An Analysis of Linked Administrative Data 2003–2015. *BMJ Open*. 12: e059242. Doi: https://doi.org/10.1136/bmjopen-2021-059242.

[3] Pola, A., Corbella, D., Righini, A., Torresin, A., Colombo, P. E., Vismara, L., Trombetta, L., Maddalo, M., Introini, M. V., Tinelli, D., Strohmenger, L., Garattini, G., Munari, A., & Triulzi, F. 2018. Computed Tomography Use in a Large Italian Region: Trend Analysis 2004-2014 of Emergency and Outpatient CT Examinations in Children and Adults. *European Radiology*. 28(6): 2308–2318. Doi: https://doi.org/10.1007/s00330-017-5225-x.

[4] Wang, R. C., Kornblith, A. E., Grupp-Phelan, J., Smith-Bindman, R., Kao, L. S., & Fahimi, J. 2021. Trends in Use of Diagnostic Imaging for Abdominal Pain in U.S. Emergency Departments. *AJR. American Journal of Roentgenology*. 216(1): 200–208. Doi: https://doi.org/10.2214/AJR.19.22667.

[5] Doria, A. S., Moineddin, R., Kellenberger, C. J., Epelman, M., Beyene, J., Schuh, S., Babyn, P. S., & Dick, P. T. 2006. US or CT for Diagnosis of Appendicitis in Children and Adults? A Meta-Analysis. *Radiology*. 241(1): 83–94. Doi: https://doi.org/10.1148/radiol.2411050913.

[6] van Eijnatten, M., van Dijk, R., Dobbe, J., Streekstra, G., Koivisto, J., & Wolff, J. 2018. CT Image Segmentation Methods for Bone used in Medical Additive Manufacturing. *Medical Engineering & Physics*. 51: 6–16. Doi: https://doi.org/10.1016/j.medengphy.2017.10.008.

[7] Fu, Y., Liu, S., Li, H., & Yang, D. 2017. Automatic and Hierarchical Segmentation of the Human Skeleton in CT images. *Physics in Medicine and Biology*. 62(7): 2812–2833. Doi: https://doi.org/10.1088/1361-6560/aa6055.

[8] Revels, J. W., Wang, S. S., Gharai, L. R., Febbo, J., Fadl, S., & Bastawrous, S. 2021. The Role of CT in Planning Percutaneous Structural Heart Interventions: Where to Measure and Why. *Clinical Imaging*. 76: 247–264. Doi: https://doi.org/10.1016/j.clinimag.2021.04.029.

[9] Li, Y., Dai, Y., Yu, N., Duan, X., Zhang, W., Guo, Y., & Wang, J. 2019. Morphological Analysis of Blood Vessels Near Lung Tumors using 3-D Quantitative CT. *Journal of X-ray Science and Technology*. 27(1): 149–160. Doi: https://doi.org/10.3233/XST-180429.

[10] Mohammed Ali, A., Hogg, P., Abuzaid, M., & England, A. 2019. Impact of Acquisition Parameters on Dose and Image Quality Optimisation in Paediatric Pelvis Radiography-A Phantom Study. *European Journal of Radiology*. 118: 130–137. Doi: https://doi.org/10.1016/j.ejrad.2019.07.014.

[11] Zhu, L., Ha, R., Machida, H., Shi, X., Wang, F., Chen, K., Chen, D., Cao, Y., Shen, Y., & Yang, L. 2023. Image Quality of Coronary CT Angiography at Ultra Low Tube Voltage Reconstructed with a Deep-learning Image Reconstruction Algorithm in Patients of Different Weight. *Quantitative Imaging in Medicine and Surgery*. 13(6): 3891–3901. Doi: https://doi.org/10.21037/qims-22-1141.

[12] Schwartz, F. R., Clark, D. P., Rigiroli, F., Kalisz, K., Wildman-Tobriner, B., Thomas, S., Wilson, J., Badea, C. T., & Marin, D. 2023. Evaluation of The Impact of a Novel Denoising Algorithm on Image Quality in Dual-energy Abdominal CT of Obese Patients. *European Radiology*. 33(10): 7056–7065. Doi: https://doi.org/10.1007/s00330-023-09644-7.

[13] Higaki, T., Nakamura, Y., Tatsugami, F., Nakaura, T., & Awai, K. 2019. Improvement of Image Quality at CT and MRI using Deep Learning. *Japanese Journal of Radiology*. 37(1): 73–80. Doi: https://doi.org/10.1007/s11604-018-0796-2.

[14] Shirasaka, T., Kojima, T., Funama, Y., Sakai, Y., Kondo, M., Mikayama, R., Hamasaki, H., Kato, T., Ushijima, Y., Asayama, Y., & Nishie, A. 2021. Image Quality Improvement with Deep Learning-based Reconstruction on Abdominal Ultrahigh-resolution CT: A Phantom Study. *Journal of Applied Clinical Medical Physics*. 22(7): 286–296. Doi: https://doi.org/10.1002/acm2.13318.

[15] Tian, Q., Li, X., Li, J., Cheng, Y., Niu, X., Zhu, S., Xu, W., & Guo, J. 2022. Image Quality Improvement in Low-dose Chest CT with Deep Learning Image Reconstruction. *Journal of Applied Clinical Medical Physics*. 23(12): e13796. Doi: https://doi.org/10.1002/acm2.13796.

[16] Barrett, J. F., & Keat, N. 2004. Artifacts in CT: Recognition and Avoidance. *Radiographics: A Review Publication of the Radiological Society of North America, Inc*. 24(6): 1679–1691. Doi: https://doi.org/10.1148/rg.246045065.

[17] Alzain, A. F., Elhussein, N., Fadulelmulla, I. A., Ahmed, A. M., Elbashir, M. E., Elamin, B. A. 2021. Common Computed Tomography Artefact: Source and Avoidance. *Egypt J Radiol Nucl Med*. 52: 151. Doi: https://doi.org/10.1186%2Fs43055-021-00530-0.

[18] Abella, M., Martinez, C., Desco, M., Vaquero, J. J., & Fessler, J. A. 2020. Simplified Statistical Image Reconstruction for X-ray CT With Beam-Hardening Artifact Compensation. *IEEE Transactions on Medical Imaging*. 39(1): 111–118. Doi: https://doi.org/10.1109/TMI.2019.2921929.

[19] Hur, J., Kim, D., Shin, Y. G., & Lee, H. 2021. Metal Artifact Reduction Method based on a Constrained Beam-hardening Estimator for Polychromatic X-ray CT. *Physics in Medicine and Biology*. 66(6): 065025. Doi: https://doi.org/10.1088/1361-6560/abe026.
[20] Abdurahman, S., Frysch, R., Bismark, R., Melnik, S., Beuing, O., & Rose, G. 2018. Beam Hardening Correction Using Cone Beam Consistency Conditions. *IEEE Transactions on Medical Imaging*. 37(10): 2266–2277. Doi: https://doi.org/10.1109/TMI.2018.2840343.
[21] Tsai, H. Y., Chen, M. C., Tsai, I. C., & Chen, C. C. 2011. Partial Ring Artifact on Cardiac CT: Image Presentation and Clinical Implication. *The International Journal of Cardiovascular Imaging*. 27(5): 689–693. Doi: https://doi.org/10.1007/s10554-011-9862-x.
[22] Sijbers, J., & Postnov, A. 2004. Reduction of Ring Artefacts in High Resolution Micro-CT Reconstructions. *Physics in Medicine and Biology*. 49(14): N247–N253. Doi: https://doi.org/10.1088/0031-9155/49/14/n06.
[23] Prell, D., Kyriakou, Y., & Kalender, W. A. 2009. Comparison of Ring Artifact Correction Methods for Flat-detector CT. *Physics in Medicine and Biology*. 54(12): 3881–3895. Doi: https://doi.org/10.1088/0031-9155/54/12/018.
[24] du Plessis, A. M., Theron, S., & Andronikou, S. 2009. The Effects of Misinterpretation of an Artefact on Multidetector Row CT Scans in Children. *Pediatric Radiology*. 39(2): 137–141. Doi: https://doi.org/10.1007/s00247-008-1052-1.
[25] Gulliksrud, K., Stokke, C., & Martinsen, A. C. 2014. How to Measure CT Image Quality: Variations in CT-numbers, Uniformity and Low Contrast Resolution for a CT Quality Assurance Phantom. *Physica Medica: PM: An International Journal Devoted to the Applications of Physics to Medicine and Biology: Official Journal of the Italian Association of Biomedical Physics (AIFB)*. 30(4): 521–526. Doi: https://doi.org/10.1016/j.ejmp.2014.01.006.
[26] Contillo, A., Veronese, A., Brombal, L., Donato, S., Rigon, L., Taibi, A., Tromba, G., Longo, R., & Arfelli, F. 2018. A Proposal for a Quality Control Protocol in Breast CT with Synchrotron Radiation. *Radiology and Oncology*. 52(3): 329–336. Doi: https://doi.org/10.2478/raon-2018-0015.
[27] IEC. 2013. International Standard IEC 61223-3-5: Evaluation and Routine Testing in Medical Imaging Departments - Part 3-5: Acceptance and Constancy Tests – Imaging Performance of Computed Tomography X-Ray Equipment.
[28] McCollough, C. H., Bruesewitz, M. R., McNitt-Gray, M. F., Bush, K., Ruckdeschel, T., Payne, J. T., Brink, J. A., Zeman, R. K., & American College of Radiology. 2004. The Phantom Portion of the American College of Radiology (ACR) Computed Tomography (CT) Accreditation Program: Practical Tips, Artifact Examples, and Pitfalls to Avoid. *Medical Physics*. 31(9): 2423–2442. Doi: https://doi.org/10.1118/1.1769632.
[29] Nowik, P., Bujila, R., Poludniowski, G., & Fransson, A. 2015. Quality Control of CT Systems by Automated Monitoring of Key Performance Indicators: A Two-Year Study. *Journal of Applied Clinical Medical Physics*. 16(4): 254–265. Doi: https://doi.org/10.1120/jacmp.v16i4.5469.
[30] Anam, C., Naufal, A., Fujibuchi, T., Matsubara, K., & Dougherty, G. 2022. Automated Development of the Contrast-detail Curve based on Statistical Low-contrast Detectability in CT Images. *Journal Of Applied Clinical Medical Physics*. 23(9): e13719. Doi: https://doi.org/10.1002/acm2.13719.
[31] Cody, D. D., Stevens, D. M., & Ginsberg, L. E. 2005. Multi-Detector Row CT Artifacts that Mimic Disease. *Radiology*. 236(3): 756–761. Doi: https://doi.org/10.1148/radiol.2363041421.
[32] Roa, A. M., Andersen, H. K., & Martinsen, A. C. 2015. CT Image Quality Over Time: Comparison of Image Quality for Six Different CT Scanners over a Six-year Period. *Journal of Applied Clinical Medical Physics*. 16(2): 4972. Doi: https://doi.org/10.1120/jacmp.v16i2.4972.
[33] Husby, E., Svendsen, E. D., Andersen, H. K., & Martinsen, A. C. T. 2017. 100 Days with Scans of the Same Catphan phantom on the Same CT Scanner. *Journal of Applied Clinical Medical Physics*. 18(6): 224–231. Doi: https://doi.org/10.1002/acm2.12186.
[34] Anam, C., Triadyaksa, P., Naufal, A., Arifin, Z., Muhlisin, Z., Setiawati, E., & Budi, W. S. 2022. Impact of ROI Size on the Accuracy of Noise Measurement in CT on Computational and ACR Phantoms. *Journal of Biomedical Physics & Engineering*. 12(4): 359–368. Doi: https://doi.org/10.31661/jbpe.v0i0.2202-1457.
[35] Hutchinson, B. D., Navin, P., Marom, E. M., Truong, M. T., & Bruzzi, J. F. 2015. Overdiagnosis of Pulmonary Embolism by Pulmonary CT Angiography. *AJR. American Journal of Roentgenology*. 205(2): 271–277. Doi: https://doi.org/10.2214/AJR.14.13938.
[36] Kheruka, S., Naithani, U., Maurya, A., Painuly, N., Aggarwal, L., & Gambhir, S. 2011. A Study to Improve the Image Quality in Low-dose Computed Tomography (SPECT) using Filtration. *Indian Journal of Nuclear Medicine: IJNM: The Official Journal of the Society of Nuclear Medicine, India*. 26(1): 14–21. Doi: https://doi.org/10.4103/0972-3919.84595.
[37] Kane, A. G., Reilly, K. C., & Murphy, T. F. 2004. Swimmer's CT: Improved Imaging of the Lower Neck and Thoracic Inlet. *AJNR. American Journal of Neuroradiology*. 25(5): 859–862.
[38] Cho, P. K., Lee, Y. H., Kim, Y. H., Choi, J. H., Shin, D. C., Choi, T. K., Kim, J. S., Kim, K. H., & Kim, S. U. 2008. Improved Imaging of the Cervico-thoracic Junction in Computed Tomography. *Yonsei Medical Journal*. 49(1): 84–89. Doi: https://doi.org/10.3349/ymj.2008.49.1.84.
[39] Habibzadeh, M. A., Ay, M. R., Asl, A. R., Ghadiri, H., & Zaidi, H. 2012. Impact of Miscentering on Patient Dose and Image Noise in X-ray CT Imaging: Phantom and Clinical Studies. *Physica Medica: PM: An International Journal Devoted to the Applications of Physics to Medicine and Biology: Official Journal of the Italian Association of Biomedical Physics (AIFB)*. 28(3): 191–199. Doi: https://doi.org/10.1016/j.ejmp.2011.06.002.
[40] Nute, J. L., Rong, J., Stevens, D. M., Darensbourg, B. J., Cheng, J., Wei, W., Hobbs, B. P., & Cody, D. D. 2013. Evaluation of over 100 Scanner-years of Computed Tomography Daily Quality Control Data. *Medical Physics*. 40(5): 051908. Doi: https://doi.org/10.1118/1.4800796.
[41] International Atomic Energy Agency. 2012. Quality Assurance Programme for Computed Tomography: Diagnostic and Therapy Applications. IAEA Human Health Series No. 19.